Improved Efficiency Optimization Control of SRM Based on Redefined Optimal Turn-On Angle and Its Corresponding Analytical Formula

Shichuan Ding, *Member, IEEE*, Xiaobin Huang, Jun Hang, *Member, IEEE*, and Wei Li, *Member, IEEE*

***Abstract*—The function analysis method based on the optimal turn-ON angle is one of the most popular efficiency optimization control strategies for switched reluctance motor (SRM) system, but it still has certain shortcomings. Under certain conditions, the optimal turn-ON angle proposed by existing research is available, but its analytical formula has either low accuracy or complex solution. In addition, when the operating condition is changed, resulting in the rising rate of the phase flux-linkage at full-voltage is less than the slope of the reference flux-linkage at θ_m, the optimal turn-ON angle proposed by the existing research will be unavailable. Hence, to solve these issues, this article presents an improved efficiency optimization control method of SRM based on a redefined optimal turn-ON angle and its corresponding analytical formula. Based on the flux-linkage analysis, the SRM system is divided into two modes according to different operating conditions, with each mode corresponding to different optimal turn-ON angles. In mode I, the optimal turn-ON angle proposed by the existing research is available and still in used. And this article presents a new analytical formula for this optimal turn-ON angle, which has high accuracy, convenient solution, and simple structural form compared to the existing analytical formulas. In mode II, the existing optimal turn-ON angle is unavailable. Thus, this article redefines a new optimal turn-ON angle in mode II and also presents its corresponding analytical formula. The analytical formulas for the two modes are similar in form and both are deduced based on the flux-linkage calculation. The simulations and experiments are conducted to verify the effectiveness of the proposed efficiency optimization control strategy.**

***Index Terms*—Analytical formula, efficiency optimization, flux-linkage, optimal turn-ON angle, switched reluctance motor.**

Received 15 April 2024; revised 8 July 2024; accepted 11 August 2024. Date of publication 21 August 2024; date of current version 7 October 2024. This work was supported in part by the National Natural Science Foundation of China under Grant 52377034 and Grant 52107034, in part by the Outstanding Youth Research Project in University of Anhui Province under Grant 2023AH020002, in part by the University Synergy Innovation Program of Anhui Province under Grant GXXT-2023-017, in part by Key Project of Excellent Young Talents in University of Anhui Province under Grant gxyqZD2021090, and in part by Anhui Provincial Major Science and Technology Project under Grant 202203c08020010. Recommended for publication by Associate Editor K.-B. Lee. *(Corresponding author: Jun Hang.)*

The authors are with the School of Electrical Engineering and Automation, Anhui University, Hefei 230601, China, and also with the National Engineering Laboratory of Energy-saving Motor and Control Technique, Anhui University, Hefei 230601, China (e-mail: 01061@ahu.edu.cn; z22301171@stu.ahu.edu.cn; junhang@ahu.edu.cn; 19804@ahu.edu.cn).

Color versions of one or more figures in this article are available at https://doi.org/10.1109/TPEL.2024.3447038.

Digital Object Identifier 10.1109/TPEL.2024.3447038

I. Introduction

SWITCHED reluctance motors (SRMs) are considered as the excellent candidates in many engineering applications, thanks to their low manufacturing cost, high reliability, and wide speed covering ranges [1], [2], [3]. Considering the special design and control strategies, SRMs are very suitable for the low-cost high-performance applications [4]. Low-efficiency operation of SRM leads to larger size, increased weight, and higher energy consumption [5]. Hence, it is desirable to achieve the efficient operation of SRM over the entire torque-speed range.

For the efficiency optimization of SRM, there has been an amount of research, which can be roughly divided into two categories: the body structure optimization design [6], [7], [8] and the efficiency optimization control [10], [11], [12], [13], [14], [15], [16], [17], [18], [19], [20], [21], [22], [23]. For a designed SRM, the latter is often adopted and is mainly dependent on the firing angle, which is the key factor in the energy conversion of SRM because it determines the relative position of the current waveform and the inductance contour [9]. At present, the efficiency optimization control strategies based on the optimal firing angle can be approximately classified as following: experimental testing method [10], [11], artificial intelligence method [5], [12], [13], online search method [14], [15], [16], and function analysis method [17], [18], [19], [20], [21], [22], [23].

Compared with other methods, the function analysis method is preferred because it avoids the drawbacks of the above methods and has efficient solution and good dynamic response. In this method, the optimal turn-ON angle is mainly discussed to optimize the efficiency of SRM, which is directly obtained through the analytical formula. And all of these analytical formulas are derived based on one feature: the optimal turn-ON angle is determined to make the peak of phase current occur at the initial overlapping position of the stator and rotor (θ_m) just right while meeting the demanded reference current, which can reduce the energy loss (copper losses) and improve the efficiency of SRM [17].

However, there are still some shortcomings in the function analysis method. The analytical formula is often established based on an ideal inductance model, where the inductance in the low-inductance region is regarded as a constant and the back electromotive force (back-EMF) is ignored accordingly. But in the actual model, the inductance in the low-inductance

region varies nonlinearly and the back-EMF cannot be ignored. This causes a certain error in the solved optimal turn-ON angle, especially when the speed is increased and the back-EMF becomes more prominent. For this, some researches have been conducted. In [18], the rough position of the optimal turn-ON angle is first found by the analytical formula based on an ideal inductance model, and then an adaptive control algorithm is added to fine-tune, which can find the optimal turn-ON angle gradually. In [19], similarly, the rough position is first found, and then an angle controller composed by two PI regulator is applied to eliminate errors, achieving automatic adjustment of turn-ON angle without the need of parameters or self-tuning techniques. In [20], [21], [22], and [23], an analytical formula based on the actual nonlinear inductance model is proposed, which fully considers the influence of the back-EMF and can directly obtain the accurate optimal turn-ON angle. These strategies mentioned in [18], [19], [20], [21], [22], and [23] can achieve good results under some operating conditions, but they still have certain drawbacks.

1) In [18], the additional online searching method (adaptive algorithm) is required for fine-tuning, which leads the optimal turn-ON angle cannot be directly obtained through an analytical formula and will inevitably bring the disadvantages of online searching method. In [19], an additional angle controller is required to eliminate error, where the optimal turn-ON angle is also not directly obtained by an analytical formula. In addition, the peak of phase current needs to be repeatedly detected and forced to occur at θ_m just right, which requires a shaft encoder for continuous monitoring. In [20], [21], [22], and [23], the optimal turn-ON angle can be directly obtained by an analytical formula, but its solution is rather complicated, which is acquired by solving the time-domain current with a first-order nonhomogeneous differential equation. And the analytical form is quite complex, where both the phase inductance and its derivative value in the low-inductance region are simultaneously required for solving.
2) Through the study, it is found that the existing optimal turn-ON angle based on the abovementioned feature (the peak of phase current occurs at θ_m just right) only holds under certain conditions. When the operating condition is changed, resulting in the rising rate of phase flux-linkage at full-voltage less than the slope of reference flux-linkage at θ_m, this feature will be invalid and the existing optimal turn-ON angle will be unavailable (the details are described in Section III).

Motivated by these, this article presents an improved efficiency optimization control method based on a redefined optimal turn-ON angle and its corresponding analytical formula. The abovementioned feature is further studied based on the flux-linkage analysis, and the SRM system is divided into two modes according to different operating conditions, with each mode corresponding to different optimal turn-ON angles. In mode I, the abovementioned feature and the optimal turn-ON angle proposed by the existing research are available, but the existing analytical formulas have either low accuracy or complex solution. Thus, this article presents a new analytical formula for this optimal turn-ON angle in mode I, being with high accuracy, simple structural form, and convenient solution. In mode II, the aforementioned feature and the existing optimal turn-ON angle are unavailable. Thus, this paper redefines a new optimal turn-ON angle in mode II and also presents its corresponding analytical formula. The analytical formulas for the two modes are similar in form and both are deduced based on the flux-linkage calculation.

II. Mathematical Model of SRM and the Optimal Turn-On Angle

A. Mathematical Model of SRM System

For the SRM system, the voltage equation for each phase can be expressed by phase flux-linkage and phase current

$$U_k = R_k \cdot i_k + \frac{\mathrm{d}\psi_k(\theta, i_k)}{\mathrm{dt}} \tag{1}$$

where the U_k is the k-phase winding terminal voltage, R_k is the resistance of k-phase winding, i_k is the k-phase current, ψ_k is the flux-linkage of k-phase, and θ is the rotor position. At constant speed, the phase voltage equation can be rewritten as

$$\begin{aligned} U_k &= R_k \cdot i_k + \frac{\partial \psi_k(\theta, i_k)}{\partial i_k}\frac{di_k}{dt} + \frac{\partial \psi_k(\theta, i_k)}{\partial \theta}\frac{d\theta}{dt} \\ &= R_k \cdot i_k + \mathrm{L_k}(\theta, i_k)\frac{\mathrm{di_k}}{\mathrm{dt}} + w\frac{\partial \mathrm{L}_k(\theta, i_k)}{\partial \theta} i_k \\ &= R_k \cdot i_k + \mathrm{L_k}(\theta, i_k)\frac{\mathrm{di_k}}{\mathrm{dt}} + e_r \end{aligned} \tag{2}$$

where L_k is the incremental inductance of k-phase winding, ω is the rotational speed, and e_r is the back-EMF. If the saturation of SRM is not considered, (2) can be simplified as

$$U_k = R_k \cdot i_k + \mathrm{L_k}(\theta)\frac{\mathrm{di_k}}{\mathrm{dt}} + w\frac{\mathrm{dL}_k(\theta)}{\mathrm{d}\theta} i_k. \tag{3}$$

The output torque of SRM is synthesized by the electromagnetic torque of each phase and can be derived as

$$T_e = \sum_{k=1}^{3} T_{ek} = \sum_{k=1}^{3} \frac{1}{2} {i_k}^2 \frac{\partial \mathrm{L_k}(i_k, \theta)}{\partial \theta} \tag{4}$$

where T_e is the output torque and T_{ek} is the electromagnetic torque of k-phase.

The efficiency of motor represents its ability to convert the electrical energy into the mechanical energy. Among the numerous efficiency optimization strategies, the maximum torque per ampere (MTPA) control is developed to maximize the torque-ampere ratio of the motor [24]. The MTPA can be achieved by reducing the phase current while keeping the output torque constant. Reducing the phase current helps the reduction of copper losses within the motor windings, thereby optimizing the efficiency of motor. Among them, the average output torque can be derived by integrating (4) over a cycle as

$$T_{\mathrm{AVG}} = \frac{1}{\theta_{sk}} \int_0^{\theta_{sk}} T_e(\theta)\, d\theta. \tag{5}$$

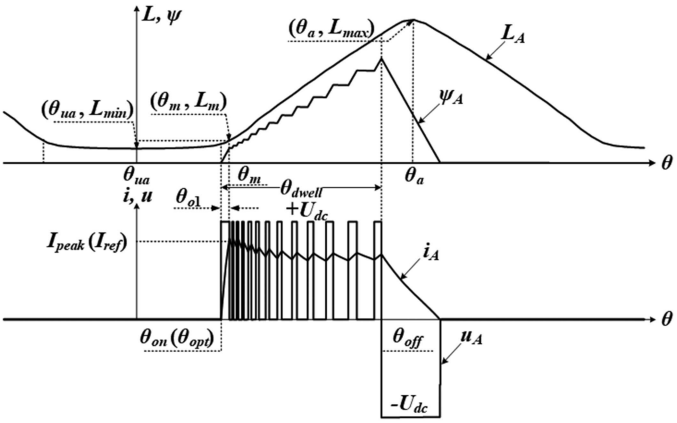

Fig. 1. Typical SRM drive waveforms with the current chopping controlled.

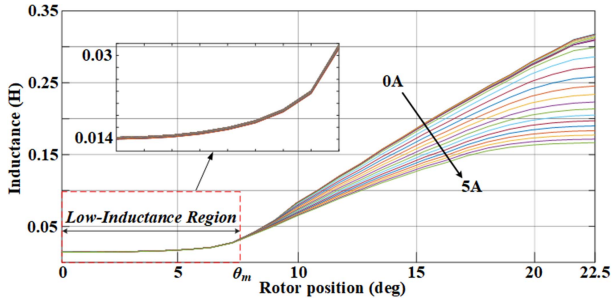

Fig. 2. Actual nonlinear inductance with phase current.

And the rms of phase current can be expressed as

$$\mathrm{I_{rms}} = \sqrt{\frac{\int_0^{\theta_{sk}} \sum_{k=1}^{3} {i_k}^2(\theta)\, d\theta}{\theta_{sk}}}. \tag{6}$$

Thus, the torque-ampere ratio of the motor can be represented by the ratio of T_{AVG} and I_{rms} as

$$\frac{\mathrm{T_{AVG}}}{I_{\mathrm{rms}}} = \frac{\frac{1}{\theta_{sk}}\int_0^{\theta_{sk}} T_e(\theta)\, d\theta}{\sqrt{\frac{\int_0^{\theta_{sk}} \sum_{k=1}^{3} {i_k}^2(\theta) d\theta}{\theta_{sk}}}}. \tag{7}$$

For a certain load condition, the average output torque T_{AVG} is essentially constant, thus, the torque-ampere ratio can be improved by reducing the I_{rms}, which in turn diminishes the copper losses and optimizes the efficiency of SRM.

B. Optimal Turn-On Angle of SRM and Related Research

The firing angle determines the relative position of the current waveform and inductance contour, which significantly affects the energy conversion of SRM. The analytical formulas of the optimal turn-ON angle are proposed in [17], [18], [19], [20], [21], [22], [23], and [24]. They are all derived based on one feature: the optimal turn-ON angle is selected to make the peak of phase current I_{peak} (i.e., the reference current I_{ref} in current chopping mode) occur at θ_m just right, as shown in Fig. 1, where an actual nonlinear inductance model is considered. L_A, ψ_A, u_A, i_A is the inductance, flux-linkage, current, and voltage profiles of A-phase winding, respectively. (θ_a, L_{max}) is the completely aligned position, (θ_{ua}, L_{min}) is the completely unaligned position, (θ_m, L_m) is the position where the stator and rotor poles start to overlap. $\theta_{\ \mathrm{ON}}$ is the turn-ON angle, $\theta_{\ \mathrm{OFF}}$ is the turn-OFF angle, θ_{opt} is the optimal turn-ON angle, θ_{o1} is the interval between $\theta_{\ \mathrm{ON}}$ and θ_m, θ_{dwell} is the conduction interval of SRM.

If the turn-ON angle is later than this defined optimal turn-ON angle (θ_{opt}), the phase current may continue to rise when the rotor enters an increasing inductance slope region, which does not make full use of the high torque output area, resulting in a decrease in SRM efficiency. Even at high speed, the phase current may not reach the reference current, causing the abnormal operation of SRM. Contrarily, if the turn-ON angle is earlier than this optimal turn-ON angle, the interval θ_{o1} will be expanded. According to the characteristics of low-inductance region and (4), the phase current conducting in this interval makes no contribution to the output torque, but increasing the copper loss and reducing the efficiency of SRM.

Based on the above analysis, the analytical formula of the optimal turn-ON angle is proposed in [17]. An ideal linear inductance model is considered, where the inductance value in the low-inductance region is regarded as a constant, and the back-EMF (e_r) in (3) is ignored accordingly. The winding voltage drop can be ignored owing to

$$R_k * i_k << \frac{d\psi_k(\theta, i_k)}{dt}. \tag{8}$$

At this time, according to (3), the phase current can increase linearly in the low-inductance region. Meanwhile, the reference current I_{ref} is required to occur at θ_m just right, so the optimal turn-ON angle θ_{opt} can be obtained as

$$\theta_{\mathrm{opt}} = \theta_{\mathrm{m}} - \theta_{\mathrm{o1}} = \theta_{\mathrm{m}} - \frac{w * \mathrm{L_{min}} * \mathrm{I}_{ref}}{\mathrm{U}_{dc}} \tag{9}$$

where the U_{dc} is the terminal voltage of dc bus.

The form is simple and the solution is convenient in (9). However, in the actual inductance model, the inductance value in the low-inductance region is not constant, as shown in Fig. 2, which is obtained by FEA and can be described as the pseudotrapezoidal inductance profile due to the fringing effect [3]. Thus, the back-EMF e_r cannot be ignored and will bring a certain error in (9). Especially at high speed, the back-EMF is more prominent and will result in a huge solving error.

In [21], focusing on the actual nonlinear inductance model, a relatively accurate analytical formula is proposed, which fully considers the influence of back-EMF. The time-domain phase current is acquired by solving the first-order nonhomogeneous differential equation in (3) and is expressed as

$$i_{\mathrm{k}}(t) = \frac{U_{dc}}{R_k + w * \frac{\mathrm{d}L_k(\theta)}{\mathrm{d}\theta}} + \left(I_0 - \frac{U_{dc}}{R_k + w * \frac{\mathrm{d}L_k(\theta)}{\mathrm{d}\theta}}\right) * e^{-\frac{R_k + w * \frac{\mathrm{d}L_k(\theta)}{\mathrm{d}\theta}}{L_k(\theta)} * \mathrm{t}}. \tag{10}$$

The initial current I_0 is equal to zero and the winding voltage drop is ignored, then the optimal turn-ON angle θ_{opt} can be obtain as

$$\theta_{\text{opt}} = \theta_{\text{m}} + \frac{L_{\text{k}}(\theta)}{\text{d}L_k(\theta)/\text{d}\theta} * \ln\left(1 - \frac{\text{w}*\text{I}_{\text{ref}}*\text{d}L_k(\theta)/\text{d}\theta}{\text{U}_{\text{dc}}}\right). \tag{11}$$

Considering the actual inductance model and the influence of back-EMF, an accurate optimal turn-ON angle is obtained by (11). However, its solution is rather complicated, which is obtained by solving the phase current in time-domain with a first-order nonhomogeneous differential equation. And compared with (9), its analytical form is more cumbersome, where the phase inductance and its derivative in the low-inductance region are simultaneously required. Besides, through the study, it is found that the solved optimal turn-ON angle will be unavailable under certain operating conditions.

Whether the solved error is large in (9), or the solution and form are complex in (11), it is because both of them obtain the optimal turn-ON angle from the perspective of phase current. But, as shown in (10), the phase current varies nonlinearly, which makes it difficult to solve the optimal turn-ON angle through phase current.

III. Proposed Optimal Turn-On Angle and its Corresponding Analytical Formula

A. Redefinition of the Optimal Turn-On Angle

The optimal turn-ON angle proposed by the existing research (as shown in Fig. 1) and its analysis seem reasonable, where the turn-ON angle is selected to make the peak of phase current occur at θ_m just right. However, the process of determining the optimal turn-ON angle lacks the quantitative analysis. There is a doubt whether there really exists a turn-ON angle that can successfully make the peak of $i_k(\theta)$ occur at θ_m just right, while meeting the demanded reference current I_{ref}. Thus, a further research based on the flux-linkage analysis is conducted.

In a closed-loop control SRM system, the load and the reference speed of SRM are usually used to depict an operating point. For a certain operating point, the demanded reference current I_{ref} can be directly obtained through speed loop and basically remains constant. Besides, it is noted from Fig. 2 that the influence of phase current on the phase inductance significantly differs around θ_m. The magnetic saturation effect is prominent after θ_m, and the current has little impact on phase inductance before θ_m. Thus, the phase inductance in the low-inductance region can be regarded as a function of rotor position only, which is expressed as $L_k(\theta)$.

For a specific position and current, the k-phase flux-linkage can be expressed as

$$\psi_{\text{k}}(\theta, \text{i}_{\text{k}}) = \text{L}_{\text{k}}(\theta, \text{i}_{\text{k}}) * \text{i}_{\text{k}}. \tag{12}$$

Thus, for a certain operating point, assuming that the reference current I_{ref} flows throughout the entire low-inductance region, the reference flux-linkage in the entire low-inductance region can be expressed as

$$\psi_{\text{ref}}(\theta, \text{I}_{\text{ref}}) = \text{L}_{\text{k}}(\theta, \text{I}_{\text{ref}}) * \text{I}_{\text{ref}} = \text{L}_{\text{k}}(\theta) * \text{I}_{\text{ref}} \tag{13}$$

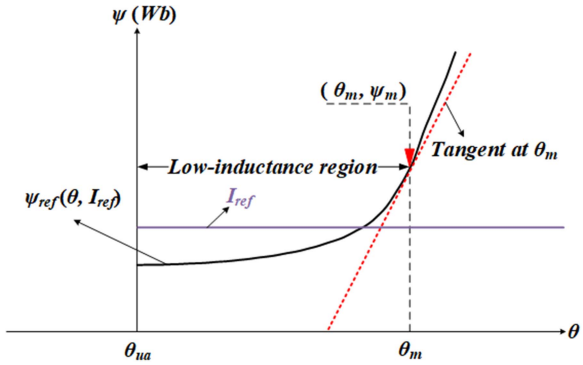

Fig. 3. Reference flux-linkage $\psi_{ref}(\theta, I_{ref})$ in low-inductance region.

where the $\psi_{ref}(\theta, I_{ref})$ is the reference flux-linkage and the second equation holds because the phase inductance in the low-inductance region is only a function of rotor position.

The contour of the $\psi_{ref}(\theta, I_{ref})$ in the low-inductance region is shown in Fig. 3. The tangent at θ_m on the curve $\psi_{ref}(\theta, I_{ref})$ is acquired as the red line. By substituting (13), the slope of this tangent can be expressed as

$$\text{k}_{tm} = \left.\frac{d\psi_{\text{ref}}(\theta, \text{I}_{\text{ref}})}{d\theta}\right|_{\theta=\theta_{\text{m}}} = \text{I}_{\text{ref}} * \left.\frac{dL_{\text{k}}(\theta)}{d\theta}\right|_{\theta=\theta_{\text{m}}}. \tag{14}$$

The voltage equation for each phase can be expressed by the phase flux-linkage in (1). Similarly, the winding voltage drop is much smaller than the $d\psi_k(\theta, i_k)/dt$ and is ignored. At a constant and nonzero speed, (1) can be expressed as

$$\frac{\text{d}\psi_k(\theta, \text{i}_{\text{k}})}{\text{d}\theta} = \frac{\text{U}_{\text{k}}}{w} \tag{15}$$

where the U_k is the k-phase winding terminal voltage and the change rate of $\psi_k(\theta, i_k)$ only depends on the U_k and w. Thus, at a constant speed, the $\psi_k(\theta, i_k)$ can be determined by simply integrating the terminal voltage U_k. Before the phase current $i_k(\theta)$ reaches its reference current I_{ref}, i.e., in the interval θ_{o1}, the phase winding is in excitation state without chopping, thus, the winding voltage U_k is always equal to the $+U_{\text{dc}}$. It means that when the SRM is in the steady-state operation, the phase flux-linkage $\psi_k(\theta, i_k)$ will grow linearly before the $i_k(\theta)$ reaches the I_{ref}, and its rising rate can be expressed as

$$\text{k}_{act} = \frac{+\text{U}_{\text{dc}}}{w}. \tag{16}$$

The rising rate k_{act} is fixed for a certain operating point. At this time, if this rising rate of the phase flux-linkage at full-voltage is larger than the slope of the tangent at θ_m, i.e., the k_{act} and k_{tm} satisfy

$$\text{k}_{act} = \frac{+\text{U}_{\text{dc}}}{w} \geq k_{\text{tm}} = \text{I}_{\text{ref}} * \left.\frac{dL_{\text{k}}(\theta)}{d\theta}\right|_{\theta=\theta_{\text{m}}} \tag{17}$$

where the k_{act} is the rising rate of the $\psi_k(\theta, i_k)$ at full-voltage and the k_{tm} is the slope of the tangent at θ_m on the curve $\psi_{ref}(\theta, I_{ref})$, it is feasible to make the peak of phase current occur at θ_m just right, and it is available to find the optimal turn-ON angle proposed by the existing research. As shown in Fig. 4, the

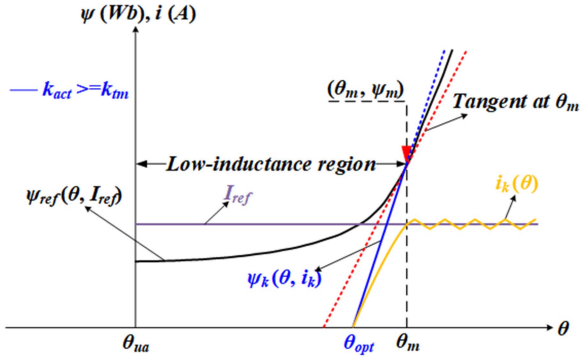

Fig. 4. Reference flux-linkage ψ_{ref} (θ, I_{ref}) intersects with the phase flux-linkage ψ_k (θ, i_k) at θ_m when $k_{act} >= k_{tm}$.

optimal turn-ON angle θ_{opt} is determined to make the $\psi_k(\theta, i_k)$ intersect with the curve ψ_{ref} (θ, I_{ref}) at θ_m, thereby the $i_k(\theta)$ can continuously grows and reaches the I_{ref} at θ_m just right.

However, if the rising rate of the phase flux-linkage at full-voltage is less than the slope of the tangent at θ_m, i.e., the k_{act} and k_{tm} satisfying

$$\mathrm{k}_{act} = \frac{+\mathrm{U}_{dc}}{w} < k_{\mathrm{tm}} = \mathrm{I}_{\mathrm{ref}} * \left.\frac{dL_{\mathrm{k}}(\theta)}{d\theta}\right|_{\theta=\theta_{\mathrm{m}}} \tag{18}$$

and the peak of phase current is required to occur at θ_m just right, as the green line shown in Fig. 5(a), another intersection between the $\psi_k(\theta, i_k)$ and the $\psi_{ref}(\theta, I_{ref})$ will be generated. The position of this intersection is defined as θ_{p1}, and the turn-ON angle is defined as θ_{on_1}. This turn-ON angle can indeed make the $\psi_k(\theta_m, i_k)$ equal to the ψ_{ref} (θ_m, I_{ref}), and the $i_k(\theta)$ can reach the I_{ref} at θ_m. However, the presence of another intersection θ_{p1} means the phase current $i_k(\theta)$ has early reached the I_{ref} at θ_{p1}. After the θ_{p1}, the winding is in the excitation state with the chopping, and the terminal voltage is no longer constant at $+U_{\mathrm{dc}}$. The $i_k(\theta)$ will remain at the I_{ref}, and the ψ_k (θ, i_k) will follow the contour of the ψ_{ref} (θ, I_{ref}) in the interval [θ_{p1}, θ_m].

Obviously, the turn-ON angle θ_{on_1} is not the optimal one, because the generated large phase current in the interval [θ_{p1}, θ_m] makes less contribution to the output torque of SRM, but increasing the copper loss and reducing the efficiency of SRM. At this time, the turn-ON angle should be considered to delay. During this process, the k_{act} is unchanged, which only depends on the speed w and the terminal voltage U_{dc}.

If the turn-ON angle is delayed to $\theta_{\mathrm{ON\_2}}$, as shown in Fig. 5(b), there is no intersection between the ψ_k (θ, i_k) and ψ_{ref} (θ, I_{ref}). It means that the ψ_k (θ, i_k) can never reach the ψ_{ref} (θ, I_{ref}), and the phase current $i_k(\theta)$ cannot reach the I_{ref} accordingly, even if the winding voltage always remains at $+U_{\mathrm{dc}}$. The current chopping will not occur, thus, the $i_k(\theta)$ can continuously grow and naturally reach its peak current near θ_m, according to (2). At this time, the SRM cannot generate sufficient output torque and cannot reach the reference speed, though the $i_k(\theta)$ can naturally reach its peak value near θ_m. Apparently, the turn-ON angle is over delayed and is not the optimal one.

As shown in Fig. 5(c), the turn-ON angle is delayed to only one intersection generated between the ψ_k (θ, i_k) and the ψ_{ref}

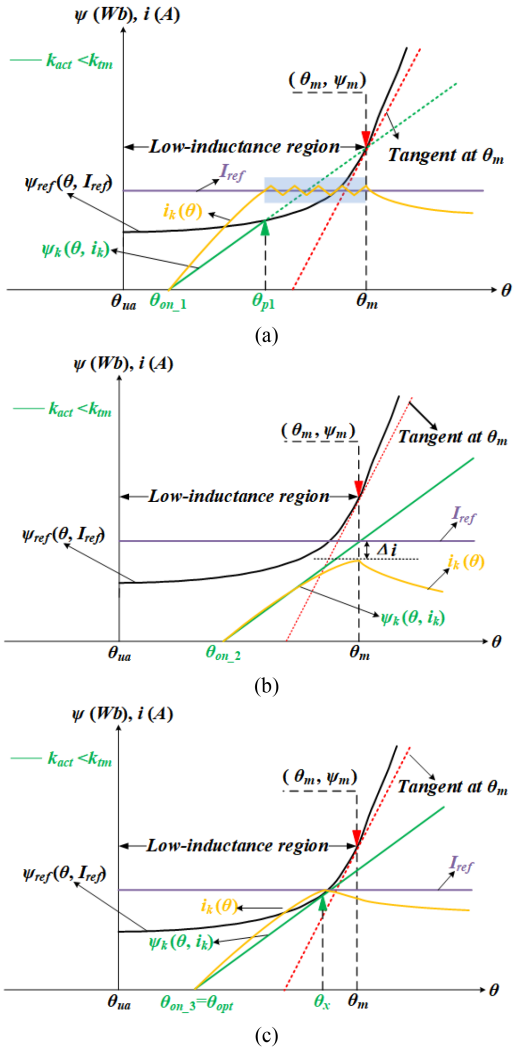

Fig. 5. Reference flux-linkage ψ_{ref} (θ, I_{ref}) and the phase flux-linkage ψ_k (θ, i_k) when $k_{act}<k_{tm}$. (a) Excessively advanced turn-ON angle. (b) Excessively delayed turn-ON angle. (c) Optimal turn-ON angle.

(θ, I_{ref}), i.e., the curve ψ_k (θ, i_k) is tangent to the ψ_{ref} (θ, I_{ref}). The position of this intersection is defined as θ_x, and the turn-ON angle is defined as $\theta_{\mathrm{ON\_3}}$. The turn-ON angle can make the ψ_k (θ_x, i_k) equal to the ψ_{ref} (θ_x, I_{ref}), and the i_k (θ) can reach the I_{ref} at θ_x accordingly. If the turn-ON angle of SRM is earlier than $\theta_{\mathrm{ON\_3}}$, the situation will be transformed into Fig. 5(a), where the $i_k(\theta)$ will reach the I_{ref} in advance and cause an energy loss in the interval [θ_{p1}, θ_x]. If the turn-ON angle of SRM is later than $\theta_{\mathrm{ON\_3}}$, the situation will be transformed into Fig. 5(b), where the $i_k(\theta)$ can never reach the I_{ref}. The turn-ON angle $\theta_{\mathrm{ON\_3}}$ satisfies

$$\theta_{\mathrm{on\_1}} < \theta_{\mathrm{on\_3}} < \theta_{\mathrm{on\_2}} \tag{19}$$

which can reduce the energy loss as much as possible while meeting the demanded reference current I_{ref}. Thus, the turn-ON angle $\theta_{\mathrm{ON\_3}}$ can be considered as the optimal turn-ON angle θ_{opt}.

Based on the above analysis, when the k_{act} and k_{tm} satisfy (17), it is available to find the optimal turn-ON angle proposed by the existing research, as shown in Fig. 4. At this time, the

SRM system is defined as mode I. When the k_{act} and k_{tm} satisfy (18), it is unavailable to find the turn-ON angle that can make the peak of the phase current occur at θ_m just right while meeting the demanded reference current I_{ref}, as shown in Fig. 5(a) and (b). At this time, the SRM system is defined as mode II. And through the study, the peak of the phase current is best to occur at θ_x, i.e., the curve $\psi_k\ (\theta,\ i_k)$ is tangent to the $\psi_{ref}\ (\theta,\ I_{ref})$ at θ_x, as shown in Fig. 5(c). The θ_x satisfies

$$\left.\frac{d\psi_{\mathrm{ref}}\left(\theta,\mathrm{I_{ref}}\right)}{d\theta}\right|_{\theta=\theta_{\mathrm{x}}}=\mathrm{I_{ref}}*\left.\frac{dL_{\mathrm{k}}\left(\theta\right)}{d\theta}\right|_{\theta=\theta_{\mathrm{x}}}=\frac{+\mathrm{U_{dc}}}{w}=\mathrm{k_{act}}. \tag{20}$$

The k_{act} in (16) and the k_{tm} in (14) depend on the designed SRM body and the working condition. For a designed SRM at a certain operating point, the k_{act} and the k_{tm} are determined. Both of them could firstly be solved through (16) and (14), and then the mode of SRM can be judged by comparing them. From a qualitative perspective, for a specific SRM, the k_{act} only depends on the reference speed w and is inversely correlated with it, while the k_{tm} only depends on the reference current I_{ref} and is positively correlated with it. The k_{act} will be decreased when the reference speed is increased and the k_{tm} will be increased when the load of SRM is increased. In other words, the $k_{act}<k_{tm}$ will be easier to be achieved and the proposed control strategy is more inclined to shifts to mode II when the load or the reference speed of SRM is increased.

B. Proposed Analytical Formula of Optimal Turn-On Angle

According to the above analysis, corresponding analytical formula of the optimal turn-ON angle should be developed to deal with these two modes. Before that, it is necessary to determine the mode of the SRM system at a certain operating point. The mode judgement of the SRM system depends on the k_{act} and k_{tm}. For the k_{act}, which is solved by (16), the $+U_{\mathrm{dc}}$ is fixed and the w can be directly acquired through the position sensor. As for the k_{tm}, the reference current I_{ref} in (14) can be directly acquired by speed loop. And the $dL_k(\theta_m)/d\theta$ in (14) depends on the structure of SRM and is fixed. Once the $dL_k(\theta_m)/d\theta$ is acquired in advance, the k_{act} and k_{tm} can be obtained in real time and the mode of SRM can be quickly determined for a certain operating point.

To judge the mode of SRM system and solve the optimal turn-ON angle later, the $dL_k(\theta)/d\theta$ in the low-inductance region should be obtained in advance. As mentioned in Fig. 2, the phase inductance in this region is only a function of rotor position, which can be expressed as the $L_k(\theta)$. The $L_k(\theta)$ can be acquired by FEA at first, and then the function fitting is applied to get the $L_k(\theta)$ and $dL_k(\theta)/d\theta$.

As shown in Fig. 6, the function fitting is applied for the $L_k(\theta)$ in the low-inductance region. After comprehensively considering the number of solved parameters and the accuracy of function fitting, the following function is adopted:

$$L_{\mathrm{k}}\left(\theta\right)=\mathrm{a}*e^{b*\theta}+c*e^{d*\theta} \tag{21}$$

where a, b, c, d are fitting parameters. The $dL_k(\theta)/d\theta$ can be obtained by differentiating (21). Once the $dL_k(\theta_m)/d\theta$ is known

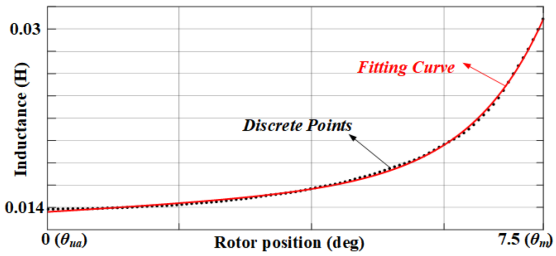

Fig. 6. Function fitting for $L_k(\theta)$.

and the mode is determined, the corresponding analytical formula of the optimal turn-ON angle should be employed.

When the SRM system enters the mode I, i.e., the k_{act} and k_{tm} satisfy (17), there is an optimal turn-ON angle that can make the peak of phase current occur at θ_m just right. The existing analytical formulas (9) and (11) can be used to acquire the optimal turn-ON angle, but they have either low accuracy or complex solution and form. For this, a new analytical formula based on the flux-linkage calculation is proposed for mode I.

According to (10), the phase current $i_k(\theta)$ grows nonlinearly before reaching the I_{ref}, so it is difficult to solve the optimal turn-ON angle through the $i_k(\theta)$. However, as mentioned in (16), the phase flux-linkage $\psi_k\ (\theta,\ i_k)$ grows linearly at a rate of $+U_{\mathrm{dc}}/w$ before the $i_k(\theta)$ reaches the I_{ref}. And before the winding is excited, the initial current I_0 and initial flux-linkage ψ_0 are equal to zero. Thus, once the phase flux-linkage at θ_m is acquired, according to (15), the interval θ_{o1} can be obtained as

$$\theta_{o1}=\theta_{\mathrm{m}}-\theta_{\mathrm{on}}=\frac{w*\left[\psi_{\mathrm{k}}(\theta_{\mathrm{m}},i_k)-\psi_0\right]}{\mathrm{U_{dc}}}=\frac{w*\psi_{\mathrm{k}}(\theta_{\mathrm{m}},i_k)}{\mathrm{U_{dc}}} \tag{22}$$

where the θ_{o1} is the interval between $\theta_{\ \mathrm{ON}}$ and θ_m, the $\psi_k\ (\theta_m,\ i_k)$ is the phase flux-linkage at θ_m.

As depicted in Fig. 4, the curve $\psi_k\ (\theta,\ i_k)$ intersects with the $\psi_{ref}\ (\theta,\ I_{ref})$ at θ_m. It means that the $i_k\ (\theta)$ can reach the I_{ref} at θ_m just right. Thus, the $\psi_k\ (\theta_m,\ i_k)$ can be further expressed as

$$\psi_{\mathrm{k}}\left(\theta_{\mathrm{m}},\mathrm{i}_k\right)=\psi_{\mathrm{k}}\left(\theta_{\mathrm{m}},\mathrm{I}_{ref}\right)=\mathrm{L_k}\left(\theta_m,\mathrm{I}_{ref}\right)*\mathrm{I}_{ref}. \tag{23}$$

By substituting (23) into (22), the optimal turn-ON angle in mode I can be obtained as

$$\theta_{\mathrm{opt}}=\theta_{\mathrm{on}}=\theta_{\mathrm{m}}-\theta_{o1}=\theta_{\mathrm{m}}-\frac{w*\mathrm{L_k}\left(\theta_m,\mathrm{I}_{ref}\right)*\mathrm{I}_{ref}}{U_{\mathrm{dc}}}. \tag{24}$$

The θ_m depends on the structure of SRM, which is fixed and known. The I_{ref} depends on the operating point and is directly obtained by the speed loop. Thus in (24), only the parameter $L_k\ (\theta_m,\ I_{ref})$ needs to be acquired. The phase inductance in the low-inductance region is only a function of rotor position, so the $L_k\ (\theta_m,\ I_{ref})$ is fixed under various operating points and can be written as a constant L_m. Hence, the analytical formula of the optimal turn-ON angle in mode I can be further written as

$$\theta_{\mathrm{opt}}=\theta_{\mathrm{m}}-\theta_{o1}=\theta_{\mathrm{m}}-\frac{w*\mathrm{L_m}*\mathrm{I}_{ref}}{U_{\mathrm{dc}}} \tag{25}$$

where L_m is the phase inductance at θ_m and is a constant, which can be acquired through (21).

Compared with (9), the proposed analytical formula in (25) has a similar analytical form. Except the parameter I_{ref}, only the parameter $L_{\min}$ is required in (9) and only the L_m is required in (25). But a more accurate optimal turn-ON angle is obtained by (25), which is derived from (1), with the consideration of the back-EMF and the actual nonlinear inductance model.

Compared with (11), the proposed analytical formula in (25) has a simple analytical form and a convenient solution, which utilizes the calculation of the linear phase flux-linkage to quickly obtain the optimal turn-ON angle, avoiding the complex calculation of the nonlinear time-domain phase current. In addition, only the parameter L_m is required in (25), but in (11), both the phase inductance value and its derivative value in the low-inductance region are required.

In general, the proposed analytical formula (25) in mode I has a high accuracy and can deal with the various operating conditions. In addition, its form is simple and its solution is convenient, being with only one parameter required.

When the SRM system satisfies (18) and enters the mode II, it is unavailable to find the turn-ON angle that can make the peak of phase current occur at θ_m just right while meeting the demanded current I_{ref}. Instead, as analyzed in Fig. 5(c), the peak of the $i_k(\theta)$ is best to occur at θ_x, which satisfies (20). For a certain operating point, the I_{ref} and k_{act} are both known. In addition, the phase inductance and its derivative in the low-inductance region are monotonic functions. Thus, by solving the inverse function of (20), the θ_x can be acquired as

$$\theta_{\mathrm{x}} = f^{-1}(\mathrm{k})\big|_{k=\mathrm{k_{act}}}, \mathrm{f}(\theta) = \frac{dL_{\mathrm{k}}(\theta)}{d\theta} * I_{ref} \tag{26}$$

where $L_k(\theta)$ can be fitted by (21). Once the θ_x is acquired, the inductance value $L_k(\theta_x)$ can also be obtained through (21).

Similar to (22), the winding voltage remains constant at the $+U_{\mathrm{dc}}$ before the θ_x, thus, the ψ_k (θ, i_k) can grow linearly at a rate of $+U_{\mathrm{dc}}/w$ before the θ_x. Once the phase flux-linkage at the θ_x is acquired, according to (15), the interval θ_{o2} can be as

$$\theta_{o2} = \theta_{\mathrm{x}} - \theta_{\mathrm{on}} = \frac{w * [\psi_{\mathrm{k}}(\theta_{\mathrm{x}}, i_k) - \psi_0]}{+\mathrm{U_{dc}}} = \frac{w * \psi_{\mathrm{k}}(\theta_{\mathrm{x}}, i_k)}{+\mathrm{U_{dc}}} \tag{27}$$

where the θ_{o2} is the interval between θ_{ON} and θ_x, the ψ_k (θ_x, i_k) is the phase flux-linkage at θ_x.

As depicted in Fig. 5(c), the curve ψ_k (θ, i_k) is tangent to the ψ_{ref} (θ, I_{ref}) at θ_x. It means that the i_k (θ) reaches the I_{ref} at θ_x just right. Thus, the ψ_k (θ_x, i_k) can be further expressed as

$$\psi_{\mathrm{k}}(\theta_{\mathrm{x}}, \mathrm{i_k}) = \psi_{\mathrm{k}}(\theta_{\mathrm{x}}, \mathrm{I}_{ref}) = \mathrm{L_k}(\theta_{\mathrm{x}}, \mathrm{I}_{ref}) * \mathrm{I}_{ref}. \tag{28}$$

By substituting (28) into (27), the optimal turn-ON angle for mode II can be obtained as

$$\theta_{\mathrm{opt}} = \theta_{\mathrm{on}} = \theta_{\mathrm{x}} - \theta_{o2} = \theta_{\mathrm{x}} - \frac{w * \mathrm{L_k}(\theta_{\mathrm{x}}, \mathrm{I}_{ref}) * \mathrm{I}_{ref}}{U_{\mathrm{dc}}}. \tag{29}$$

The L_k (θ_x, I_{ref}) is also a function of rotor position only since the θ_x is still less than the θ_m. Once the θ_x is determined, the L_k (θ_x, I_{ref}) is certain and can be written as a constant L_x as well. Thus, the analytical formula of the optimal turn-ON angle

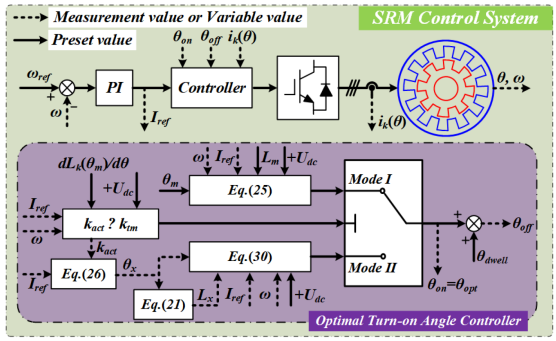

Fig. 7. Control block diagram of optimal turn-ON angle for SRM system.

TABLE I
SPECIFICATIONS PARAMETERS OF SRM

Rotor pole number	8	Stator pole number	12
Phase number	3	Rated speed (r/min)	1500
Stator pole arc (°)	14	Rotor pole arc (°)	16
Rated current (A)	4.2	Rated torque (N.m)	4.77
Rated voltage (V)	220	Rated power (W)	750

in mode II can be further written as

$$\theta_{\mathrm{opt}} = \theta_{\mathrm{x}} - \theta_{o2} = \theta_{\mathrm{x}} - \frac{w * \mathrm{L_x} * \mathrm{I}_{ref}}{U_{\mathrm{dc}}} \tag{30}$$

where L_x is the phase inductance at θ_x and is a constant, which can also be acquired through (21).

The analytical form of (30) is the same as that of (25), and the deduction process are similar. Both of them are derived based on the flux-linkage calculation. The only difference is the intersection changes from θ_m in (25) to θ_x in (30). Once satisfying (17), the analytical formula in (30) can transform into (25). Therefore, the two analytical formulas for these two modes can be regarded as one analytical formula to a certain extent. But one more step is adopted to find the θ_x through (26) in mode II. The whole control block diagram of the optimal turn-ON angle for the SRM system is shown in Fig. 7.

IV. SIMULATION RESULTS AND ANALYSIS

To validate the effectiveness of the proposed optimal turn-ON angle and its corresponding analytical formula, the simulation is studied in the MATLAB/Simulink. And the conventional analytical formulas (9) and (11) are established to make a comparison. The parameters of SRM are shown in Table I and the following angles are expressed in mechanical angles. The completely unaligned position of the SRM (θ_{ua}) is defined as the 0-degree position, where the phase inductance is at the minimum value, as shown in Fig. 1. The initial overlapping position (θ_m) is equal to 7.5 degree (°), which is obtained according to the structure of the SRM. The conduction interval (θ_{dwell}) is fixed at 12.5°, which is selected with a comprehensive consideration after conducting a lot of simulations and experiments under various working conditions. According to (7), under same load, the I_{rms} in different method are used to make a comparison. In addition, the efficiency (η) of the SRM is also recorded to verify

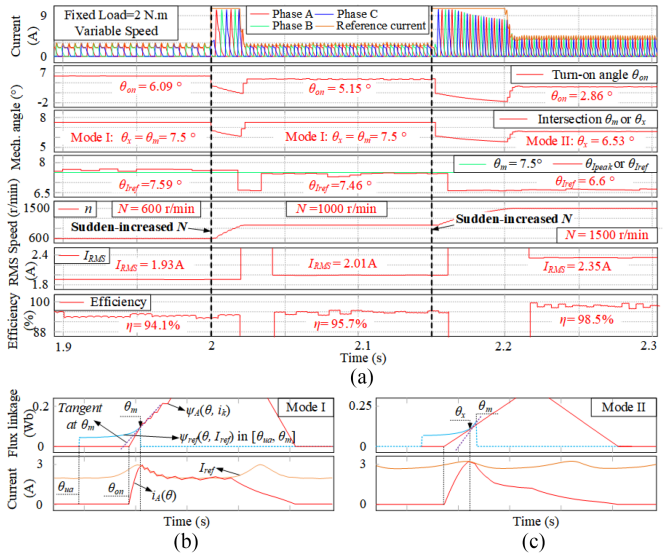

Fig. 8. Simulation results of variable speed with the optimal turn-ON angle obtained by the proposed analytical formula. (a) N from 600 r/min to 1000 r/min, from 1000 r/min to 1500 r/min. (b) Local enlarged $\psi_k(\theta,i_k)$ and $i_k(\theta)$ at 600 r/min. (c) Local enlarged $\psi_k(\theta,i_k)$ and $i_k(\theta)$ at 1500 r/min.

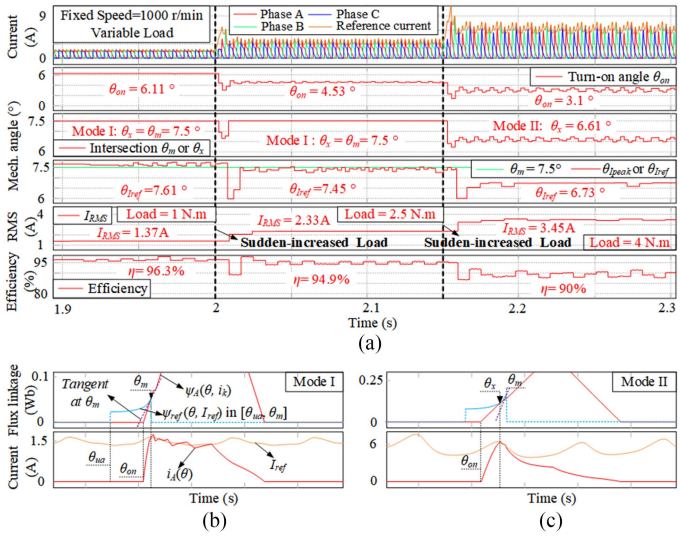

Fig. 9. Simulation results of variable load with the optimal turn-ON angle obtained by the proposed analytical formula. (a) Variable load from 1 N.m to 2.5 N.m, from 2.5 N.m to 4 N.m. (b) Local enlarged $\psi_k(\theta,i_k)$ and $i_k(\theta)$ at 1 N.m. (c) Local enlarged $\psi_k(\theta,i_k)$ and $i_k(\theta)$ at 4 N.m.

the effectiveness of the proposed method. The η is determined by the ratio of output power to input power, where the output power is the product of the motor's speed and torque, and the input power is the output power of the dc power supply.

In Fig. 8, the variable speed simulation is conducted with the optimal turn-ON angle obtained by the proposed analytical formula. As shown in Fig. 8(a), the load is fixed at 2 N.m and the reference speed (N) is set to 600 r/min before t = 2 s. In this operating point, the k_{act} and k_{tm} satisfy (17) and the SRM enters the mode I. The optimal turn-ON angle obtained by (25) satisfies $\theta_{opt} = 6.09°$ and the position where the $i_k(\theta)$ reaches the I_{ref} just right satisfies $\theta_{Iref} = 7.59°$. As shown in Fig. 8(b), the optimal turn-ON angle can make the ψ_k (θ, i_k) reach the ψ_{ref} (θ, I_{ref}) near θ_m, and the $i_k(\theta)$ can reach the I_{ref} near θ_m accordingly. Meanwhile, the rms of phase current satisfies $I_{\rm rms} = 1.93$ A and the efficiency of the SRM satisfies $\eta = 94.1\%$.

At the moment t = 2 s, the N is changed from 600 r/min to 1000 r/min. When the speed is in a stable state, the SRM is still in mode I. The θ_{opt} is equal to 5.15°, which can also make the $i_k(\theta)$ reach the I_{ref} near θ_m ($\theta_{Iref} = 7.46°$). The $I_{\rm rms}$ and the η in this operating point satisfy $I_{\rm rms} = 2.01$ A and $\eta = 95.7\%$.

At the moment t = 2.15 s, the N is changed from 1000 r/min to 1500 r/min. When the SRM is in a stable state, the k_{act} and k_{tm} satisfy (18) and the SRM enters the mode II. The turn-ON angle that makes the θ_{Iref} occur at θ_m just right cannot be found. Instead, the redefined optimal turn-ON angle obtained by (30) satisfies $\theta_{opt} = 2.86°$. And the $i_k(\theta)$ satisfies $\theta_{Iref} = 6.6°$, which is close to the solved θ_x (6.53°) by (26). As shown in Fig. 8(c), the θ_{opt} can make the ψ_k (θ, i_k) reach ψ_{ref} (θ, I_{ref}) near θ_x, and the $i_k(\theta)$ can reach I_{ref} near θ_x. Under this operating point, the $I_{\rm rms}$ is equal to 2.35 A and the η is equal to 98.5%. It can be seen that when the N is increased, the rising speed of $i_k(\theta)$ will slow down, causing the interval θ_{o1} obtained by (22) to enlarge and the θ_{opt} obtained by (25) to advance. Meanwhile, it should be noted that the peak current is slightly higher than the reference current, which is mainly caused by the hysteresis regulator.

In Fig. 9, the variable load simulation is conducted with the optimal turn-ON angle obtained by the proposed analytical formula. As shown in Fig. 9(a), the N is fixed at 1000 r/min and the load is set to 1 N.m before t = 2 s. The k_{act} and k_{tm} satisfy (17) and the SRM system enters the mode I. The optimal turn-ON angle obtained by (25) satisfies $\theta_{opt} = 6.11°$ and the $i_k(\theta)$ satisfies $\theta_{Iref} = 7.61°$. As the local enlarged images shown in Fig. 9(b), the θ_{opt} can make the $\psi_k(\theta, i_k)$ reach the ψ_{ref} (θ, I_{ref}) near θ_m, and the $i_k(\theta)$ can reach I_{ref} near θ_m. The $I_{\rm rms}$ and the η in this operating point satisfy $I_{\rm rms} = 1.37$ A and $\eta = 96.3\%$.

At the moment t = 2 s, the load of SRM is changed to 2.5 N.m. The k_{act} and k_{tm} satisfy (17) and the SRM is still in mode I. The θ_{opt} is equal to 4.53°, which also makes the $i_k(\theta)$ reach the I_{ref} near θ_m ($\theta_{Iref} = 7.45°$). The $I_{\rm rms}$ and the η in this operating point satisfy $I_{\rm rms} = 2.33$ A and $\eta = 94.9\%$.

At the moment t = 2.15 s, the load of SRM is changed to 4 N.m. The redefined optimal turn-ON angle obtained by (30) satisfies $\theta_{opt} = 3.1°$. The $i_k(\theta)$ satisfies $\theta_{Iref} = 6.73°$, which is close to the solved θ_x (6.61°) by (26). As shown in Fig. 9(c), the optimal turn-ON angle can make the ψ_k (θ, i_k) reach ψ_{ref} (θ, I_{ref}) near θ_x, and the $i_k(\theta)$ can reach I_{ref} near θ_x. The $I_{\rm rms}$ and the η in this operating point satisfy $I_{\rm rms} = 3.45$ A and $\eta = 90\%$. It is seen that when the load is enlarged, the I_{ref} will be increased, causing the interval θ_{o2} obtained by (27) to enlarge and the θ_{opt} obtained by (30) to advance.

For comparison, under the same operating conditions, the simulations are conducted based on the turn-ON angle obtained by the conventional analytical formulas (9) and (11).

In Fig. 10(a), the simulation of variable speed is conducted with the analytical formula (9) adopted. When the speed is stable

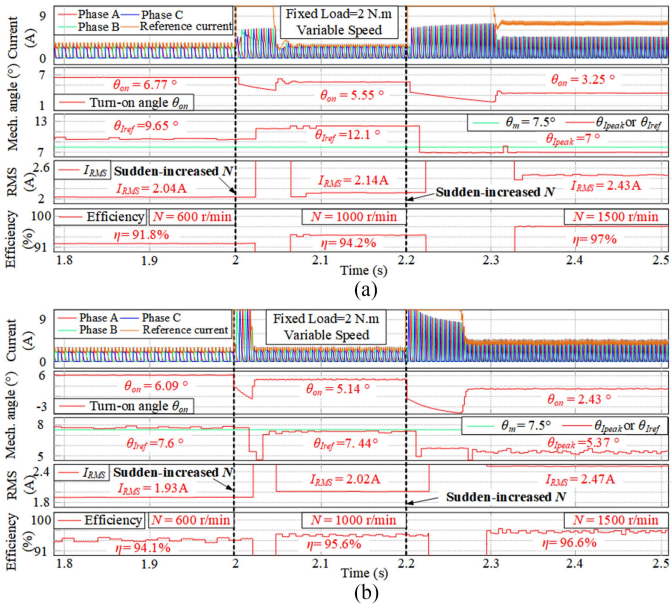

Fig. 10. Simulation results of variable speed with the optimal turn-ON angle obtained by the conventional analytical formula. (a) Obtained by (9). (b) Obtained by (11).

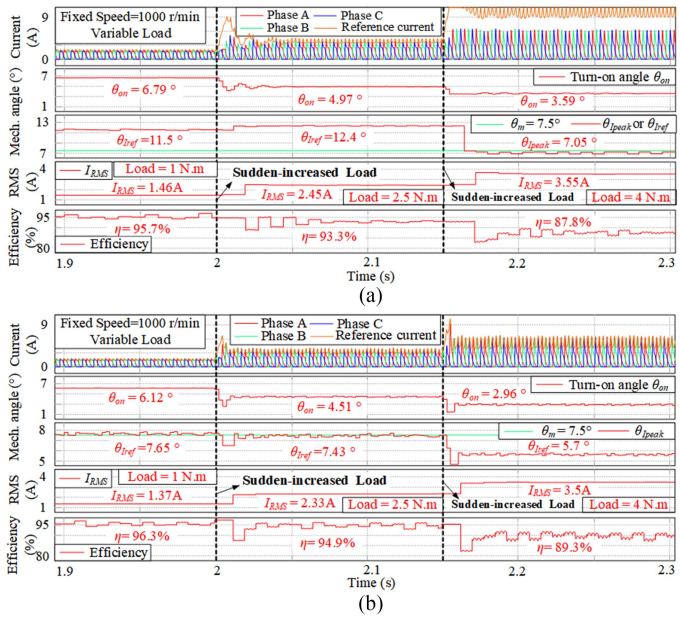

Fig. 11. Simulation results of variable load with the turn-ON angle obtained by the conventional analytical formulas. (a) Obtained by (9). (b) Obtained by (11).

at 600 r/min, these results are acquired as: $\theta_{\text{ON}} = 6.77°$, $\theta_{Iref} = 9.65°$, $I_{\text{rms}} = 2.04$ A and $\eta = 91.8\%$. When the speed is stable at 1000 r/min, these results are acquired as: $\theta_{\text{ON}} = 5.55°$, $\theta_{Iref} = 12.1°$, $I_{\text{rms}} = 2.14$ A and $\eta = 94.2\%$. These turn-ON angles make the $i_k(\theta)$ reach the I_{ref} at a position exceeding θ_m and cannot achieve the MTPA of SRM. When the N is changed to 1500 r/min, these results are acquired as: $\theta_{\text{ON}} = 3.25°$, $\theta_{I\text{peak}} = 7°$, $I_{\text{rms}} = 2.43$ A, and $\eta = 97\%$. The solved turn-ON angle is over delayed, which makes the SRM enter the situation mentioned in Fig. 5(b) and the $i_k(\theta)$ can never reach I_{ref}. At this time, the current chopping will not occur, and the $i_k(\theta)$ can continuously grow and naturally reach its peak near θ_m. But the SRM still cannot generate sufficient torque and reach the reference speed N.

In Fig. 10(b), the simulation of variable speed is conducted with the analytical formula (11) adopted. When the speed is stable at 600 r/min, these results are acquired as: $\theta_{\text{ON}} = 6.09°$, $\theta_{Iref} = 7.6°$, $I_{\text{rms}} = 1.93$ A, and $\eta = 94.1\%$. When the speed is stable at 1000 r/min, these results are acquired as: $\theta_{\text{ON}} = 5.14°$, $\theta_{Iref} = 7.44°$, $I_{\text{rms}} = 2.02$ A, and $\eta = 95.6\%$. These results are basically consistent with those obtained by the proposed analytical formula and the solved turn-ON angle can successfully make the $i_k(\theta)$ reach I_{ref} near θ_m, which aligns with the theoretical analysis for the SRM in Mode I. When the speed is stable at 1500 r/min, the simulation results are acquired as: $\theta_{\text{ON}} = 2.43°$, $\theta_{Iref} = 5.37°$, $I_{\text{rms}} = 2.47$ A, and $\eta = 96.6\%$. This solved turn-ON angle makes the $i_k(\theta)$ reach I_{ref} in advance, because another intersection (θ_{p1}) between the ψ_k (θ, i_k) and the ψ_{ref} (θ, I_{ref}) is generated, as the situation mentioned in Fig. 5(a). At this time, the generated large phase current in the interval [θ_{p1}, θ_m] will cause an energy loss and reduce the efficiency of SRM.

In Fig. 11, the simulation of variable load is conducted with the conventional analytical formulas. In Fig. 11(a), the turn-ON angle obtained by (9) is adopted. When the load of SRM is equal to 1 N.m or 2.5 N.m, the solved turn-ON angle makes the $i_k(\theta)$ reach I_{ref} at a position exceeding θ_m and cannot achieve the MTPA of SRM. When the load is adjusted to 4 N.m, the turn-ON angle makes the SRM enter the situation depicted in Fig. 5(b), where the $i_k(\theta)$ can never reach I_{ref} and the SRM cannot reach the N. In Fig. 11(b), the turn-ON angle obtained by (11) is adopted. When the load is equal to 1 N.m or 2.5 N.m, the solved turn-ON angle is basically consistent with that obtained by the proposed analytical formula, and the i_k (θ) can reach I_{ref} near θ_m. When the load is adjusted to 4 N.m, the solved turn-ON angle makes the $i_k(\theta)$ reach I_{ref} in advance and causes an energy loss, as the situation depicted in Fig. 5(a).

Under various operating conditions, the above simulation results are compared and listed in the Table II. All in all, the turn-ON angle obtained by (9) is over delayed due to the ignorance of back-EMF. The solved angle will make the $i_k(\theta)$ reach I_{ref} at a position exceeding θ_m and cannot achieve the MTPA control of SRM. Moreover, it is easy to fall into the situation in Fig. 5(b) and the SRM cannot operate normally. The optimal turn-ON angle obtained by (11) can be accurate in mode I, but it has complex solution and form. Besides, when the SRM enters the mode II, it is easy to fall into the situation in Fig. 5(a), where the $i_k(\theta)$ will reach I_{ref} in advance and cause an energy loss. By the proposed analytical formula, the solved turn-ON angle can make the $i_k(\theta)$ reach I_{ref} at θ_m or θ_x with a low error under any operating conditions, and the efficiency of the SRM can be improved owing to the reduction of copper losses. From the Table II, compared to the conventional methods, the I_{rms} is

TABLE II
SIMULATION RESULTS COMPARISON

Operating condition	Method	θ_{on} (°)	θ_{Iref} (°)	I_{RMS} (A)	η (%)	Mode
600 r/min 2 N.m	Proposed	6.09	7.59	1.93	94.1	I
	Eq. (9)	6.77	9.65	2.04	91.8	
	Eq. (11)	6.09	7.6	1.93	94.1	
1000 r/min 2 N.m	Proposed	5.15	7.46	2.01	95.7	I
	Eq. (9)	5.55	12.1	2.14	94.2	
	Eq. (11)	5.14	7.44	2.02	95.6	
1500 r/min 2 N.m	Proposed	2.86	6.6 (θ_x=6.53)	2.35	98.5	II
	Eq. (9)	Fail to operate normally in Fig. 10(a)				
	Eq. (11)	2.43	5.37	2.47	96.7	
1 N.m 1000 r/min	Proposed	6.11	7.61	1.37	96.3	I
	Eq. (9)	6.79	11.5	1.46	95.7	
	Eq. (11)	6.12	7.65	1.37	96.3	
2.5 N.m 1000 r/min	Proposed	4.53	7.45	2.33	94.9	I
	Eq. (9)	4.97	12.4	2.45	93.3	
	Eq. (11)	4.51	7.43	2.34	94.8	
4 N.m 1000 r/min	Proposed	3.1	6.73 (θ_x=6.61)	3.45	90	II
	Eq. (9)	Fail to operate normally in Fig. 11(a)				
	Eq. (11)	2.96	5.7	3.5	89.3	

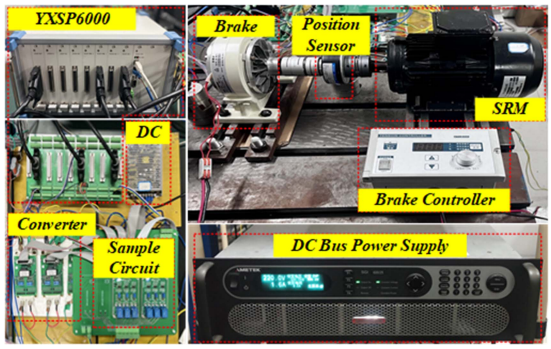

Fig. 12. Experiment platform.

less and the η is higher in the proposed analytical formula for a certain working point, which means a more accurate optimal turn-ON angle is solved. In addition, it can be observed that the SRM is more likely to shifts to mode II when the load or the reference speed of SRM is increased, which is consistent with the above theoretical analysis.

V. EXPERIMENTAL RESULTS ANALYSIS

To further validate the effectiveness of the proposed optimal turn-ON angle and its corresponding analytical formula, an experimental platform is established, as shown in Fig. 12. Similarly, the conventional analytical formulas (9) and (11) are utilized to make a comparison. The parameters of SRM are listed in Table I and the setting parameters are the same as those in the simulation. The asymmetric half-bridge power converter is

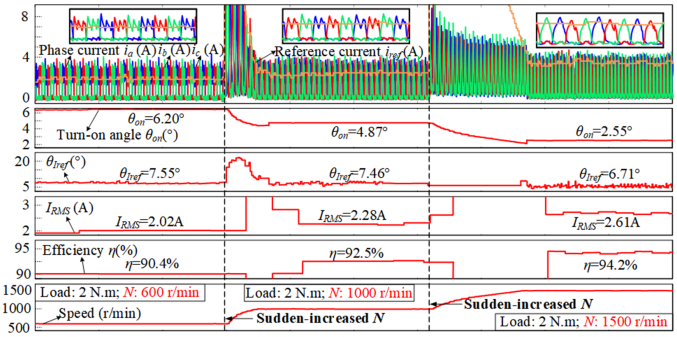

Fig. 13. Experimental results of variable speed with the optimal turn-ON angle obtained by proposed analytical formula.

adopted and the terminal voltage of dc bus ($U_{\rm dc}$) is set to the rated voltage of SRM (220 V). A magnetic powder brake with an accuracy of 0.127 N.m/div is selected as the load, which can be adjusted by the brake controller. The phase current signals and the position signals of SRM are acquired by the current sample circuit and the position sensor, respectively. All of these signals are sent to the YXSP6000 controller for processing and generating all control commands.

The results of variable speed experiment with the turn-ON angle obtained by the proposed analytical formula are shown in Fig. 13. The load is fixed at 2 N.m and the reference speed (N) is changed from 600 r/min to 1000 r/min, from 1000 r/min to 1500 r/min. At 600 r/min and 1000 r/min, the k_{act} and k_{tm} satisfy (17) and the SRM is in mode I. When the speed is stable at 600 r/min, the optimal turn-ON angle obtained by (25) satisfies $\theta_{opt} = 6.20°$ and the position where the $i_k(\theta)$ reaches I_{ref} just right satisfies $\theta_{Iref} = 7.55°$. When the speed is stable at 1000 r/min, the optimal turn-ON angle obtained by (25) satisfies $\theta_{opt} = 4.87°$ and the $i_k(\theta)$ satisfies $\theta_{Iref} = 7.46°$. These obtained turn-ON angles can successfully make the $i_k(\theta)$ reach the I_{ref} near θ_m. In addition, at 600 r/min, the $I_{\rm rms}$ and η are 2.02 A and 90.4%, respectively, and at 1000 r/min, they are 2.28 A and 92.5%, respectively. When the N continues to increase and the speed is stable at 1500 r/min, the SRM enters mode II as the k_{act} drops and the SRM satisfies (18). It can be seen from the enlarged phase current image that there is almost no current chopping in SRM, which aligns with the theoretical analysis in Mode II. The optimal turn-ON angle obtained by (30) satisfies $\theta_{opt} = 2.55°$ and the $i_k(\theta)$ satisfies $\theta_{Iref} = 6.71°$. The $I_{\rm rms}$ and the η in this operating point satisfy $I_{\rm rms} = 2.61$ A and $\eta = 94.2\%$.

For comparison, variable speed experiments are conducted based on the turn-ON angle obtained by conventional analytical formulas (9) and (11) under the same operating conditions.

The results of variable speed experiment with the turn-ON angle obtained by (9) are shown in Fig. 14. The load is fixed at 2 N.m and the N is changed from 600 r/min to 1000 r/min, from 1000 r/min to 1500 r/min. When the speed is stable at 600 r/min, the experiment results are acquired as: $\theta_{\rm ON} = 6.68°$, $\theta_{Iref} = 8.47°$, $I_{\rm rms} = 2.07$ A, and $\eta = 89.5\%$. When the speed is stable at 1000 r/min, the experiment results are acquired as: $\theta_{\rm ON} = 5.38°$, $\theta_{Iref} = 10.45°$, $I_{\rm rms} = 2.37$ A, and $\eta = 91.2\%$. Obviously, these

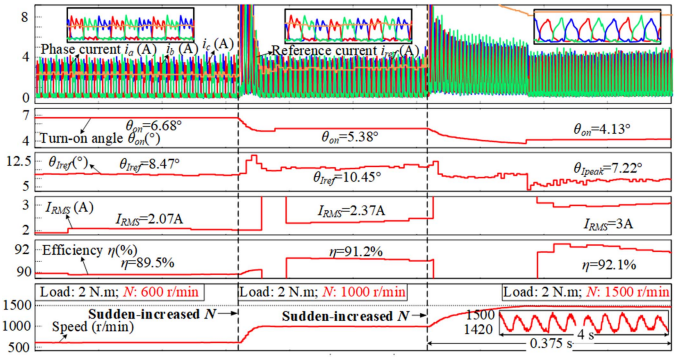

Fig. 14. Experimental results of variable speed with the turn-ON angle obtained by (9).

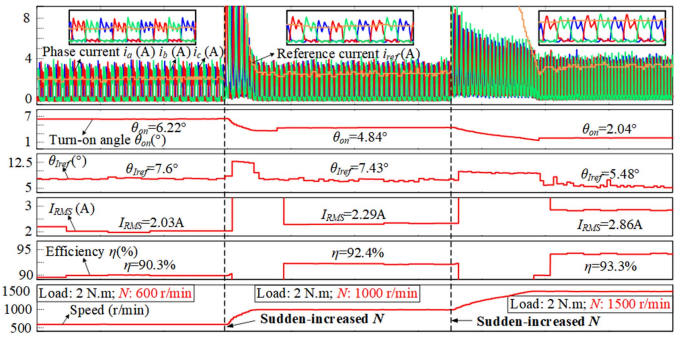

Fig. 15. Experimental results of variable speed with the turn-ON angle obtained by (11).

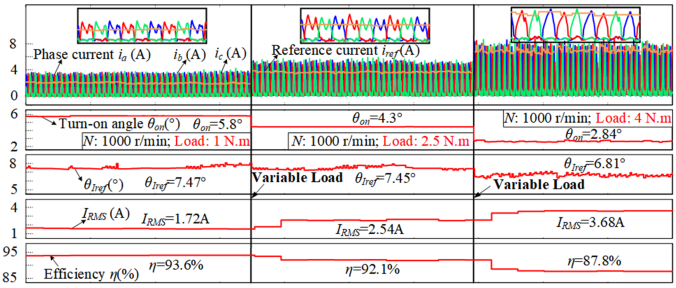

Fig. 16. Experimental results of variable load with the turn-ON angle obtained by the proposed analytical formula.

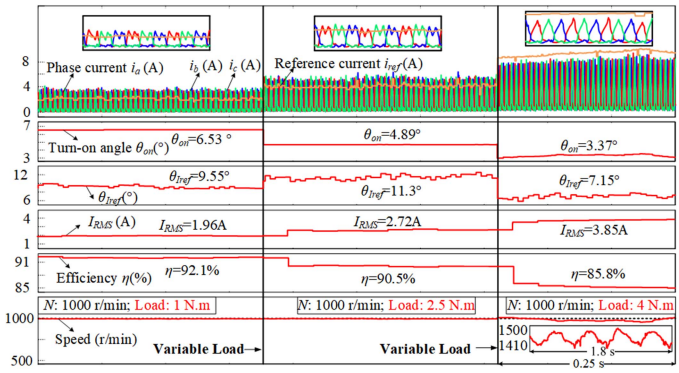

Fig. 17. Experimental results of variable load with the turn-ON angle obtained by (9).

obtained turn-ON angles are over delayed, which make the $i_k(\theta)$ reach I_{ref} at a position exceeding θ_m and cannot achieve the MTPA of SRM. When the speed is low, the error of the optimal turn-ON angle is small. But when the speed increases, the error enlarges rapidly and the efficiency drops sharply. When the N is increased to 1500 r/min, the results are acquired as follows: $\theta_{\text{ON}} = 4.13°$, $\theta_{I\text{peak}} = 7.22°$, $I_{\text{rms}} = 3$ A, and $\eta = 92.1\%$. In this operating point, it can be seen from the local enlarged images that the obtained turn-ON angle cannot make the $i_k(\theta)$ reach I_{ref}, and the speed of SRM cannot stably reach the reference speed, causing the abnormal operation of SRM, as the situation depicted in Fig. 5(b).

The results of variable speed experiment with the turn-ON angle obtained by (11) are shown in Fig. 15. The N is changed from 600 r/min to 1000 r/min, from 1000 r/min to 1500 r/min, with the load fixed at 2 N.m. When the speed is stable at 600 r/min, the experiment results are acquired as: $\theta_{\text{ON}} = 6.22°$, $\theta_{Iref} = 7.6°$, $I_{\text{rms}} = 2.03$ A, and $\eta = 90.3\%$. When the speed is stable at 1000 r/min, the experiment results are acquired as: $\theta_{\text{ON}} = 4.84°$, $\theta_{Iref} = 7.43°$, $I_{\text{rms}} = 2.29$ A, and $\eta = 92.4\%$. In these two operating points, as the theoretical analysis in Mode I, these obtained turn-ON angles are basically consistent with those obtained by the proposed formula, and the $i_k(\theta)$ can successfully reach I_{ref} near θ_m. When the N continues to increase and the speed is stable at 1500 r/min, the experiment results are acquired as: $\theta_{\text{ON}} = 2.04°$, $\theta_{Iref} = 5.48°$, $I_{\text{rms}} = 2.86$ A, and $\eta = 93.3\%$. The solved turn-ON angle makes the $i_k(\theta)$ reach I_{ref} in advance and causes an energy loss in vain, as the situation depicted in Fig. 5(a).

The results of variable load experiment with the turn-ON angle obtained by the proposed analytical formula are shown in Fig. 16. The N is fixed at 1000 r/min and the load are 1 N.m, 2.5 N.m, and 4 N.m, respectively. The results of steady-state operation stage are recorded and the dynamic stage are ignored, as that is not our focus and takes up a large space of the figure. When the load of SRM is set to 1 N.m or 2.5 N.m, the SRM system enters mode I. The obtained optimal turn-ON angle at 1 N.m satisfies $\theta_{opt} = 5.8°$ and the $i_k(\theta)$ can reach the I_{ref} near θ_m ($\theta_{Iref} = 7.47°$). The obtained optimal turn-ON angle at 2.5 N.m satisfies $\theta_{opt} = 4.3°$ and the $i_k(\theta)$ can also reach the I_{ref} near θ_m ($\theta_{Iref} = 7.45°$). At 1 N.m, the I_{rms} and η are 1.72 A and 93.6%, respectively, and at 2.5 N.m, they are 2.54 A and 92.1%, respectively. When the load is adjusted to 4 N.m, the SRM system enters mode II. As the local enlarged current waveform shown, there is almost no current chopping in SRM as well. The turn-ON angle obtained by (30) satisfies $\theta_{opt} = 2.84°$ and the $i_k(\theta)$ satisfies $\theta_{Iref} = 6.81°$. At this time, the I_{rms} and η are 3.68 A and 87.8%, respectively.

Similarly, for comparison, the variable load experiment with the turn-ON angle obtained by (9) is conducted and shown in Fig. 17. The N is fixed at 1000 r/min and the load are 1 N.m, 2.5 N.m, and 4 N.m, respectively. When the load of SRM is set to 1 N.m or 2.5 N.m, the solved turn-ON angle makes the $i_k(\theta)$ reach I_{ref} at a position exceeding θ_m and cannot achieve the

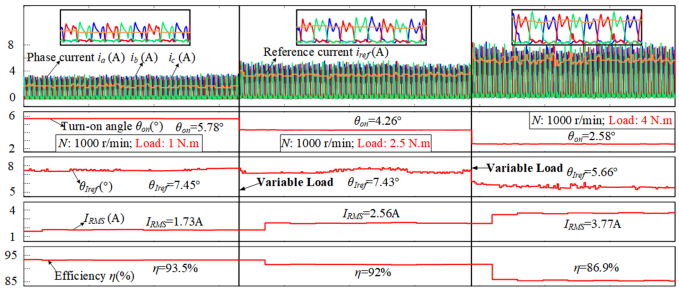

Fig. 18. Experimental results of variable load with the turn-ON angle obtained by (11).

TABLE III
EXPERIMENTAL RESULTS COMPARISON

Operating condition	Method	θ_{on} (°)	θ_{Iref} (°)	I_{RMS} (A)	η (%)	Mode
600 r/min 2 N.m	Proposed	6.2	7.55	2.02	90.4	I
	Eq. (9)	6.68	8.47	2.07	89.5	
	Eq. (11)	6.22	7.6	2.03	90.3	
1000 r/min 2 N.m	Proposed	4.87	7.46	2.28	92.5	I
	Eq. (9)	5.38	10.45	2.37	91.2	
	Eq. (11)	4.84	7.43	2.29	92.4	
1500 r/min 2 N.m	Proposed	2.55	6.71	2.61	94.2	II
	Eq. (9)	Fail to operate normally in Fig. 14				
	Eq. (11)	2.04	5.48	2.86	93.3	
1 N.m 1000 r/min	Proposed	5.8	7.47	1.72	93.6	I
	Eq. (9)	6.53	9.55	1.96	92.1	
	Eq. (11)	5.78	7.45	1.73	93.5	
2.5 N.m 1000 r/min	Proposed	4.3	7.45	2.54	92.1	I
	Eq. (9)	4.89	11.3	2.72	90.5	
	Eq. (11)	4.26	7.43	2.56	92	
4 N.m 1000 r/min	Proposed	2.84	6.81	3.68	87.8	II
	Eq. (9)	Fail to operate normally in Fig. 17				
	Eq. (11)	2.58	5.66	3.77	86.9	

MTPA of SRM. When the load is adjusted to 4 N.m, the turn-ON angle makes the SRM enter the situation depicted in Fig. 5(b), where the $i_k(\theta)$ cannot reach I_{ref} and the SRM fails to operate normally, as the local enlarged waveform shown.

In Fig. 18, the variable load experiment with the turn-ON angle obtained by (11) is conducted. The N is fixed at 1000 r/min and the load are 1 N.m, 2.5 N.m, and 4 N.m, respectively. When the load is equal to 1 N.m or 2.5 N.m, the solved turn-ON angle is basically consistent with that obtained by the proposed analytical formula, and the i_k (θ) can reach I_{ref} near θ_m. When the load is adjusted to 4 N.m, the results are acquired as: $\theta_{\text{ON}} = 2.58°$, $\theta_{Iref} = 5.66°$, $I_{\text{rms}} = 3.77$ A, and $\eta = 86.9\%$. The solved turn-ON angle makes the $i_k(\theta)$ reach I_{ref} in advance and causes an energy loss, as the situation depicted in Fig.5(a).

The experimental results based on the turn-ON angle obtained by the proposed analytical formula and conventional methods are compared and are listed in the Table III. Same conclusion can be drawn: the turn-ON angle obtained by (9) is over delayed, which cannot achieve the MTPA control of SRM and even causing the abnormal operation of SRM when it falls into the situation in Fig. 5(b). The turn-ON angle obtained by (11) can also find the optimal turn-ON angle in mode I, but it has complex solution and form. Besides, it is easy to fall into the situation in Fig. 5(a) when the working condition is changed and the SRM enters mode II. At this time, the $i_k(\theta)$ will reach I_{ref} in advance and cause an energy loss. By the proposed analytical formula, the obtained turn-ON angle can make the $i_k(\theta)$ reach I_{ref} at θ_m or θ_x with low error under any operating conditions, and reduce the energy loss as much as possible. From the Table III, compared to the conventional methods, the I_{rms} is less and the η is higher in the proposed analytical formula for a certain working point, which means a more accurate optimal turn-ON angle is solved. And it also shows that the SRM system is more likely to shifts to mode II when the load or the reference speed of SRM is increased. In addition, it can be seen from the Table II and the Table III that there is a certain difference between the simulation results and the experiment results, which is primarily due to the difference between the actual SRM model and the simulated SRM model built. And the factors such as iron loss, mechanical loss are ignored in the simulation, which also causes the difference of the results. In addition, calculation accuracy, measurement errors, and environmental factors will all affect the simulation and experimental results differently.

VI. CONCLUSION

Focusing on the drawbacks of the optimal turn-ON angle of SRM and its analytical formula in the existing research, this article presents an improved efficiency optimization control method of SRM based on a redefined optimal turn-ON angle and its corresponding analytical formula. On the basis of flux-linkage analysis, the SRM system is divided into two modes according to different operating conditions, with each mode corresponding to different optimal turn-ON angles. Through theoretical analysis, simulations and experiments verification, the following conclusions are drawn.

1) The SRM enters mode I when the k_{act} and k_{tm} satisfy (17), where the existing optimal turn-ON angle is available. But the existing analytical formula of this optimal turn-ON angle has either low accuracy or complex solution. The presented analytical formula in this article can obtain this optimal turn-ON angle with low error, thereby reducing the energy loss and improving the efficiency of SRM. Meanwhile, its solution is convenient and its form is simple, which avoids the complex calculation of nonlinear phase current and utilizes the linear flux-linkage in θ_{o1} to quickly obtain the optimal turn-ON angle.
2) The SRM enters mode II when the k_{act} and k_{tm} satisfy (18), where the existing optimal turn-ON angle is unavailable as it either causes an energy loss in vain or prevents the SRM from operating normally. The redefined optimal turn-ON angle for mode II in this article makes the peak of the $i_k(\theta)$ occur at θ_x, which can reduce the energy loss as much as possible. The corresponding analytical formula

for mode II is also presented in this article, which can solve the redefined optimal turn-ON angle accurately. In addition, the analytical formulas for the two modes are similar in form, and both are deduced based on the fast flux-linkage calculation.

REFERENCES

[1] S. Song, G. Fang, Z. Zhang, R. Ma, and W. Liu, "Unsaturated-inductance-based instantaneous torque online estimation of switched reluctance machine with locally linearized energy conversion loop," *IEEE Trans. Ind. Electron.*, vol. 65, no. 8, pp. 6109–6119, Aug. 2018.

[2] C. Gan, F. Meng, Z. Yu, R. Qu, Z. Liu, and J. Si, "Online calibration of sensorless position estimation for switched reluctance motors with parametric uncertainties," *IEEE Trans. Power Electron.*, vol. 35, no. 11, pp. 12307–12320, Nov. 2020.

[3] S. Rani and R. Jayapragash, "FEA-based geometrical modification of switched reluctance motor for radial force reduction," *Chin. J. Electr. Eng.*, vol. 10, no. 1, pp. 124–135, Mar. 2024.

[4] Y. Hu, W. Ding, T. Wang, S. Li, S. Yang, and Z. Yin, "Investigation on a multimode switched reluctance motor: Design, optimization, electromagnetic analysis, and experiment," *IEEE Trans. Ind. Electron.*, vol. 64, no. 12, pp. 9886–9895, Dec. 2017.

[5] J. Xiu, S. Wang, and Y. Xiu, "Optimum firing angles control for switched reluctance motor based on IPSO at steady state," *IEEE Trans. Energy Convers.*, vol. 38, no. 2, pp. 780–788, Jun. 2023.

[6] T. Raminosoa, B. Blunier, D. Fodorean, and A. Miraoui, "Design and optimization of a switched reluctance motor driving a compressor for a PEM fuel-cell system for automotive applications," *IEEE Trans. Ind. Electron.*, vol. 57, no. 9, pp. 2988–2997, Sep. 2010.

[7] B. Anvari, H. A. Toliyat, and B. Fahimi, "Simultaneous optimization of geometry and firing angles for in-wheel switched reluctance motor drive," *IEEE Trans. Transport. Electrific.*, vol. 4, no. 1, pp. 322–329, Mar. 2018.

[8] S.-H. Mao and M.-C. Tsai, "A novel switched reluctance motor with c-core stators," *IEEE Trans. Magn.*, vol. 41, no. 12, pp. 4413–4420, Dec. 2005.

[9] K. I. Hwu and C. M. Liaw, "Intelligent tuning of commutation for maximum torque capability of a switched reluctance motor," *IEEE Trans. Energy Convers.*, vol. 18, no. 1, pp. 113–120, Mar. 2003.

[10] M. Pittermann, J. Fort, J. Diesl, and V. Pavlicek, "Optimal SRM-control algorithm to achieve maximum torque and real converter limits," in *Proc. Int. Conf. Mechatron. - Mechatronika*, Brno, Czech Republic, 2018, pp. 1–8.

[11] Y. Sozer and D. A. Torrey, "Optimal turn-off angle control in the face of automatic turn-on angle control for switched-reluctance motors," *IET Electric Power Appl.*, vol. 1, no. 3, pp. 395–401, Mar. 2007.

[12] C. Xia, F. Jia, M. Xue, and H. Fang, "Commutation signal identification for switched reluctance motors based on fuzzy neural networks," in *Proc. IEEE Int. Conf. Autom. Logistics*, Qingdao, China, 2008, pp. 700–704.

[13] B. Fan, Y. Liu, Y. Li, and Z. Zhou, "Optimized control of SRG based on fuzzy logic by turn-on and turn-off angle," in *Proc. IEEE Int. Conf. Aircr. Utility Syst.*, Beijing, China, 2016, pp. 82–86.

[14] X. D. Xue et al., "Optimal control method of motoring operation for SRM drives in electric vehicles," *IEEE Trans. Veh. Tech.*, vol. 59, no. 3, pp. 1191–1204, Mar. 2010.

[15] S. Ali, R. Amir, A. Milad, and N. Seyyed Mortaza Saghaian, "Commutation angles adjustment in SRM drives to reduce torque ripple below the motor base speed," *Turkish J. Electr. Eng. Comput. Sci.*, vol. 24, no. 2: pp. 669–682, Oct. 2016.

[16] P. C. Kjaer, P. Nielsen, L. Andersen, and F. Blaabjerg, "A new energy optimizing control strategy for switched reluctance motors," *IEEE Tran. Ind. Appl.*, vol. 31, no. 5, pp. 1088–1095, Sep./Oct. 1995.

[17] B. K. Bose, T. J. E. Miller, P. M. Szczesny, and W. H. Bicknell, "Microcomputer control of switched reluctance motor," *IEEE Tran. Ind. Appl.*, vol. IA-22, no. 4, pp. 708–715, Jul. 1986.

[18] C. Mademlis and I. Kioskeridis, "Performance optimization in switched reluctance motor drives with online commutation angle control," *IEEE Trans. Energy Convers.*, vol. 18, no. 3, pp. 448–457, Sep. 2003.

[19] Y. Sozer, D. A. Torrey, and E. Mese, "Automatic control of excitation parameters for switched-reluctance motor drives," *IEEE Trans. Power Electron.*, vol. 18, no. 2, pp. 594–603, Mar. 2003.

[20] Y. Z. Xu, R. Zhong, L. Chen, and S. L. Lu, "Analytical method to optimise turn on angle and turn off angle for switched reluctance motor drives," *IET Electric Power Appl.*, vol. 6, no. 9, pp. 593–603, Jul. 2012.

[21] H. Mahmoud and S. László, "A new technique for optimum excitation of switched reluctance motor drives over a wide speed range," *Turkish J. Electr. Eng. Comput. Sci.*, vol. 26, no. 5: pp. 2753–2767, Sep. 2018.

[22] L. A. Quraan, F. Al-Amyal, and S. Laszlo, "Adaptive firing angles control for switched reluctance motor," in *Proc. IEEE Int. Conf. Workshop Obuda Electr. Power Eng.*, Budapest, Hungary, 2021, pp. 119–124.

[23] G. Singh and B. Singh, "An analytical approach for optimizing commutation strategy of switched reluctance motor drive for light electric vehicle," in *Proc. IEEE Int. Conf. Power Electron., Smart Grid Renewable Energy*, Cochin, India, 2020, pp. 1–6.

[24] H. Hadla and F. Santos, "Performance comparison of field-oriented control, direct torque control, and model-predictive control for SynRMs," *Chin. J. Electr. Eng.*, vol. 8, no. 1, pp. 24–37, Mar. 2022.

Shichuan Ding (Member, IEEE) received the B.Sc. degree in automation from Anhui University, Hefei, China, in 2001, the M.Sc. degree in nuclear science and technology from the University of Science and Technology of China, Hefei, China, in 2006, and the Ph.D. degree in electrical engineering from Southeast University, Nanjing, China, in 2018.

Since 2001, he has been with Anhui University, where he is currently a Professor. He was a Research Scholar with WEMPEC in University of Wisconsin Madison from 2015 to 2016. In recent years, he has authored and coauthored more than 30 technical papers. His research interests include electrical machine drive, power electronics applications, and energy management in EVs and in power system.

Xiaobin Huang received the B.Sc. degree in electrical engineering and automation from Wenzhou University, Wenzhou, China, in 2022. He is currently working toward the M.Sc. degree in electrical engineering with Anhui University, Hefei, China.

His current research interest includes advance control of electrical machine.

Jun Hang (Member, IEEE) received the B.Sc. and M.Sc. degrees in electrical engineering from Anhui University of Science and Technology, Huainan, China, in 2008 and 2011, respectively, and the Ph.D. degree in electrical engineering from Southeast University, Nanjing, China, in 2016.

From April to July 2015, he was a joint Ph.D. student with the Department of Energy Technology, Aalborg University, Denmark. Since 2016, he has been with Anhui University, Hefei, China, where he is currently a Professor with the School of Electrical Engineering and Automation. In recent years, he has authored and coauthored more than 30 technical papers. His current research interests include condition monitoring, fault diagnosis, permanent magnet machine, and renewable energy.

Dr. Hang was the recipient of the 1st Prize of 2016 Student Thesis Contest (Ph.D. Category), IEEE Industry Applications Society.

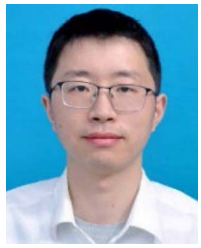

Wei Li (Member, IEEE) received the B.Sc. degree from Anhui University of Technology, Ma'anshan, China, in 2008, the M.E. degree from Anhui University, Hefei, China, in 2012, and the Ph.D. degree from the School of Electrical Engineering, Southeast University, Nanjing, China, in 2019.

Since 2019, he has been with Anhui University, Hefei, China, where he is currently a Lecturer. His current research interests include the reliability of permanent magnet machines for application in hybrid vehicles.